Target Tracking Using Monopulse MIMO Radar With Distributed Antennas*

Sandeep Gogineni, *Student Member, IEEE* and Arye Nehorai*, *Fellow, IEEE*
Department of Electrical and Systems Engineering
Washington University in St. Louis
One Brookings Drive, St. Louis, MO 63130, USA

Email: {sgogineni, nehorai}@ese.wustl.edu
Phone: 314-935-7520 Fax: 314-935-7500

***Abstract*—We propose a Multiple Input Multiple Output (MIMO) radar system with distributed antennas that employs monopulse processing at the receivers. We also propose an algorithm to track a moving target using this system. This algorithm is simple and practical to implement. It efficiently combines the information present in the local estimates of the receivers. Since most modern tracking radars already use monopulse processing at the receiver, the proposed system does not need much additional hardware. Using numerical simulations, we demonstrate the advantages of the proposed system over conventional single antenna monopulse radar. We also show that the proposed algorithm keeps track of rapidly maneuvering airborne and ground targets.**

I. Introduction

A radar transmitter sends an electro-magnetic signal which bounces off the surface of the target and travels in space towards the receiver. When the electro-magnetic signal reflects from the surface of the target, it undergoes an attenuation which depends on the radar cross section (RCS) of the target. This RCS varies with the angle of view of the target. We can exploit these angle dependent fluctuations by employing widely separated antennas [1]–[4]. When viewing the target from different angles simultaneously, the angles which result in a low RCS value are compensated by the others which have a higher RCS, thereby leading to an overall improvement in the performance of the radar system. This is the motivation for using Multiple Input Multiple Output (MIMO) radar with distributed antennas. Apart from distributed antenna configuration, MIMO radar has also been suggested for use in a colocated antenna configuration [5], [6]. Such a system exploits the flexibility of transmitting different waveforms from different elements of the array. In this paper, we will only be dealing with MIMO radar in the context of distributed antennas.

Most of the tracking radars have separate range tracking systems that keep track of the range (distance) of the target and sends only signals coming from the desired range gate to the angle tracking system [7]. The range tracker has an estimate of the time intervals when the target returns are expected. The focus of this paper however is on the angle tracking system, the most common form of which is the monopulse radar [8]–[11]. In monopulse, we project the radar beams slightly to either side of the radar axis in both the angular dimensions (azimuth and elevation) [8], [9]. The beams are generated simultaneously. Hence, monopulse radar is immune to pulse-to-pulse target fluctuations. We compare the received signals in each of these beams to keep track of the angular position of the target. To perform this comparison, the system computes a ratio which is a function of the signals received through these beams. This ratio is called Monopulse Ratio. Most modern radars use monopulse processors. There are two types of monopulse tracking radars in use; amplitude-comparison and phase-comparison. In amplitude-comparison monopulse, the beams originate from the same phase center whereas the beams in a phase-comparison monopulse system are parallel to each other and originate from slightly shifted phase centers. Essentially, the signals received from both the beams have the same phase in amplitude-comparison monopulse and they differ only in the amplitude. However, for phase-comparison monopulse systems, the exact opposite is true. In this paper, whenever we refer to monopulse, we mean amplitude-comparison monopulse. Later in this paper (also [12]), we propose a radar system that combines the advantages of monopulse and distributed MIMO radar. It provides the spatial diversity offered by MIMO radar with widely separated antennas and is also immune to highly fluctuating target returns just like any monopulse tracking radar.

The rest of this paper is organized as follows. In section II, we propose a monopulse MIMO radar system and describe its structure in detail. In section III, we describe the signal model of our proposed system. In section IV, we propose a tracking algorithm for this monopulse MIMO radar system. We describe the various steps involved in tracking the location of the target. In section V, we use numerical simulations to demonstrate the improvement in performance offered by this proposed system over conventional Single Input Single Output (SISO) monopulse systems. We also show that the proposed algorithm keeps track of an airborne target even when it maneuvers quickly and changes directions. Further, we

⋆This work was supported by the Department of Defense under the Air Force Office of Scientific Research MURI Grant FA9550-05-1-0443 and ONR Grant N000140810849.

∗Corresponding author

978-1-4244-5813-4/10/$26.00 ©2010 IEEE

demonstrate that the proposed radar system efficiently keeps track of a ground target that changes directions at sharp angles. Finally, in section VI, we conclude this paper.

II. System Description

In this section, we give a brief description of our proposed system. Fig. 1 gives the basic structure of our monopulse MIMO radar system. The system has M transmit antennas and N receive antennas. The different transmitters illuminate the target from multiple angles and the reflected signals from the surface of the target are captured by widely separated receivers. All the receivers are connected to a fusion center which can be a separate block by itself or one of the receivers can function as the fusion center. Before initializing the tracking process, the fusion center makes the boresight axes of all the receivers point towards the same point in space. The fusion center has knowledge of the exact locations of all the transmit and receive antennas and hence it can direct the receivers to align their respective axes accordingly.

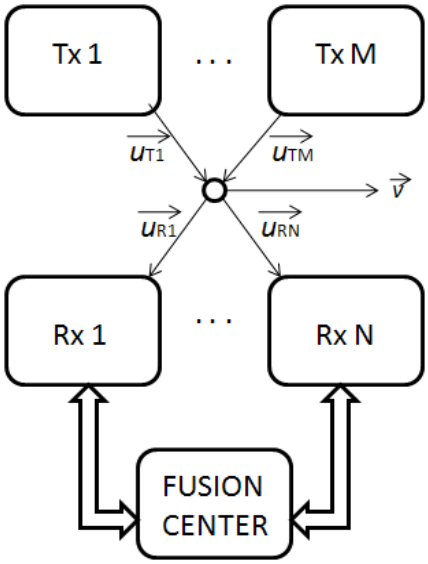

Fig. 1. Our proposed monopulse MIMO radar system.

Each of the receivers generates two overlapping receive beams on either side of the boresight axis (see Fig. 2). In this paper, we assume that the target moves only in the azimuth plane scanned by these beams. However, we can easily extend this to the other angular dimension (elevation) without loss of generality by adding the extra beams. We compare the signals arriving through the two beams at each of the receivers in order to update the estimate of the angular position of the target and subsequently update the location of the boresight axis. All the receivers send their new local angular estimates to the fusion center. The fusion center makes use of all the information sent to it and makes a final global decision on the location where the target could be present. It instructs all the receivers to align their boresight axes towards this estimated target location.

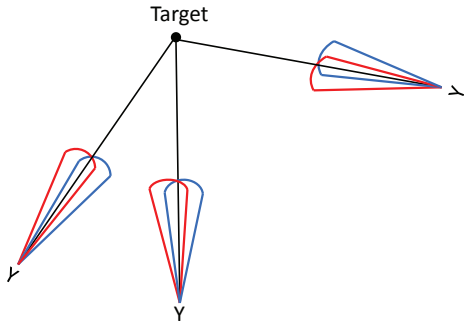

Fig. 2. Monopulse MIMO radar receivers.

III. Signal Model

A. Transmitted Waveforms

Let $\widetilde{s}_i(t), i = 1, \ldots, M$, denote the complex baseband waveform transmitted from the i^{th} antenna. Therefore, after modulation, the bandpass signal emanating from the i^{th} transmit antenna is given as

$$s_i(t) = \mathrm{Re}\left\{\widetilde{s}_i(t) e^{j2\pi f_c t}\right\}, \tag{1}$$

where f_c denotes the carrier frequency. We assume that $\widetilde{s}_i(t)$ are narrowband waveforms with pulse duration T seconds and are repeated once every T_{R} seconds. We do not impose any further constraints on these waveforms. Especially, note that we do not need orthogonality between the different transmitted waveforms unlike conventional MIMO radar with widely separated antennas. As we shall see later in the paper, the reason for this is that we do not need a mechanism to separate these waveforms at the receivers. We process the sum of the signals coming from different transmitters collectively without separating them. This is another advantage of the proposed system because the assumption that the waveforms remain orthogonal for different delays and doppler shifts is unrealistic. In section V (numerical results), we considered rectangular pulses.

B. Target and Received Signals

We assume a far-field point target with its RCS varying with the angle of view. Let $a_{ik}(t)$ denote the complex attenuation factor due to the distance of travel and the target RCS for the signal transmitted from the i^{th} transmitter and reaching the k^{th} receiver and τ_{ik} is the corresponding time delay. Note that for a colocated MIMO system, $a_{ik}(t)$ for different transmitter-receiver pairs will be the same because all the antennas will be viewing the target from closely spaced angles. Different models have been proposed in literature to model the time varying fluctuations in these attenuations $a_{ik}(t)$ [13]–[15]. Some of these models incorporate pulse-to-pulse fluctuations, scan-to-scan fluctuations, etc. These correspond to fast moving and slow moving targets respectively. In our numerical simulations, we consider a rapidly fluctuating scenario where these attenuations keep varying from one pulse instant to another because of the motion of the target. We assume $a_{ik}(t)$ to be constant over the duration of one pulse. These attenuations

$a_{ik}(t)$ are not known at the receivers. Under the narrowband assumption for the complex envelopes of the transmitted waveforms, and further assuming the target velocity to be much smaller than the speed of propagation of the wave in the medium, the bandpass received waveform is

$$y_k(t) = \sum_{i=1}^{M} \mathrm{Re}\left\{ a_{ik}(t)\widetilde{s}_i(t-\tau_{ik}) e^{j2\pi(f_c(t-\tau_{ik})+f_{Dik}(t-\tau_{ik}))} \right\}, \quad (2)$$

where f_{Dik} is the Doppler shift along the path from the i^{th} transmitter to the k^{th} receiver,

$$f_{Dik} = \frac{f_c}{c}\left(\langle \overrightarrow{\boldsymbol{v}}, \overrightarrow{\boldsymbol{u}}_{Rk} \rangle - \langle \overrightarrow{\boldsymbol{v}}, \overrightarrow{\boldsymbol{u}}_{Ti} \rangle \right), \quad (3)$$

where $\overrightarrow{\boldsymbol{v}}, \overrightarrow{\boldsymbol{u}}_{Ti}, \overrightarrow{\boldsymbol{u}}_{Rk}$ denote the target velocity vector, unit vector from the i^{th} transmitter to the target and the unit vector from the target to the k^{th} receiver, respectively; $\langle , \rangle$ is the inner product operator, and c is the speed of propagation of the wave in the medium. Equation (2) is valid only when the target is moving with constant velocity.

C. Beamforming

The receive beams are generated using Capon beamformers [16]. Capon beamformer is the minimum variance distortionless spatial filter. Each receiver generates two beams located at the same phase center using two linear arrays. Each array has L elements, each separated by a uniform distance of $\frac{\lambda}{2}$, where $\lambda = \frac{c}{f_c}$ is the wavelength corresponding to the carrier. Under the given antenna spacing, the steering vector of the beamformers becomes

$$\boldsymbol{d}(\theta, f) = \left[1, e^{-j\pi\frac{f\lambda}{c}\cos\theta}, \ldots, e^{-j(L-1)\pi\frac{f\lambda}{c}\cos\theta}\right]^T, \quad (4)$$

where $[\cdot]^T$ denotes the transpose. Let θ_k be the angle between

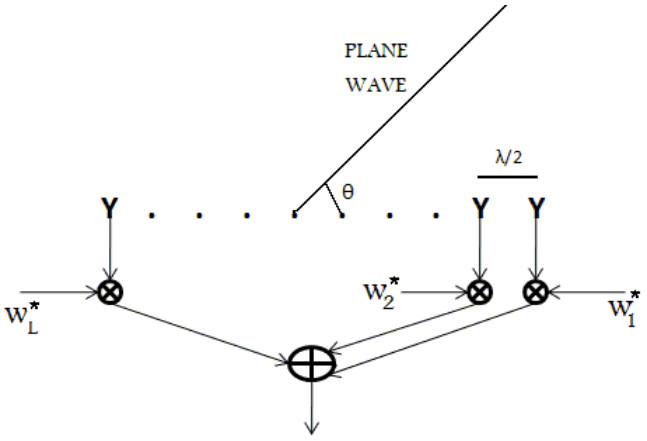

Fig. 3. Spatial beamformer at the receiver.

the approaching plane wave and the two linear arrays at the k^{th} receiver (see Fig. 3). The received signals are first demodulated before passing through the two beamformers. Define the outputs of the two beamformers as $y_k^{\mathrm{l}}(t)$ and $y_k^{\mathrm{r}}(t)$, where the superscripts l and r correspond to the left and the right beams, respectively. Also, let $\boldsymbol{w}_k^{\mathrm{l}} = \left[w_{k1}^{\mathrm{l}}, \ldots, w_{kL}^{\mathrm{l}}\right]^T$ and $\boldsymbol{w}_k^{\mathrm{r}} = \left[w_{k1}^{\mathrm{r}}, \ldots, w_{kL}^{\mathrm{r}}\right]^T$ denote the corresponding weight vectors of the beamformers. Similarly, $\boldsymbol{e}_k^{\mathrm{l}}(t) = \left[e_{k1}^{\mathrm{l}}(t), \ldots, e_{kL}^{\mathrm{l}}(t)\right]^T$ and $\boldsymbol{e}_k^{\mathrm{r}}(t) = \left[e_{k1}^{\mathrm{r}}(t), \ldots, e_{kL}^{\mathrm{r}}(t)\right]^T$ are the additive noise vectors of these two spatial filters. Defining

$$x_k(t) \triangleq \sum_{i=1}^{M} a_{ik}(t)\widetilde{s}_i(t-\tau_{ik}) e^{j2\pi(f_c(-\tau_{ik})+f_{Dik}(t-\tau_{ik}))}, \quad (5)$$

and sampling the outputs of the spatial filters, we get

$$y_k^{\mathrm{l}}[n] = x_k[n]\left(\boldsymbol{w}_k^{\mathrm{l}}\right)^H \boldsymbol{d}(\theta_k, f_c + f_{Dik}) + \left(\boldsymbol{w}_k^{\mathrm{l}}\right)^H \boldsymbol{e}_k^{\mathrm{l}}[n] \quad (6)$$

$$y_k^{\mathrm{r}}[n] = x_k[n]\left(\boldsymbol{w}_k^{\mathrm{r}}\right)^H \boldsymbol{d}(\theta_k, f_c + f_{Dik}) + \left(\boldsymbol{w}_k^{\mathrm{r}}\right)^H \boldsymbol{e}_k^{\mathrm{r}}[n] \quad (7)$$

We assume that the additive noise vectors at the two arrays of sensors have zero mean and covariance matrices $\boldsymbol{R}_k^{\mathrm{l}}$ and $\boldsymbol{R}_k^{\mathrm{r}}$, respectively. The Capon beamformer creates the beams by minimizing $\left(\boldsymbol{w}_k^{\mathrm{l}}\right)^H \boldsymbol{R}_k^{\mathrm{l}} \boldsymbol{w}_k^{\mathrm{l}}$ and $\left(\boldsymbol{w}_k^{\mathrm{r}}\right)^H \boldsymbol{R}_k^{\mathrm{r}} \boldsymbol{w}_k^{\mathrm{r}}$ subject to the constraints $\left\{\left(\boldsymbol{w}_k^{\mathrm{l}}\right)^H \boldsymbol{d}(\theta_k^{\mathrm{l}}, f_c) = 1\right\}$ and $\left\{\left(\boldsymbol{w}_k^{\mathrm{r}}\right)^H \boldsymbol{d}(\theta_k^{\mathrm{r}}, f_c) = 1\right\}$, respectively. The solution to this optimization problem gives the weights of the beamformers [17]

$$\boldsymbol{w}_k^{\mathrm{l}} = \frac{\left(\boldsymbol{R}_k^{\mathrm{l}}\right)^{-1} \boldsymbol{d}(\theta_k^{\mathrm{l}}, f_c)}{\boldsymbol{d}(\theta_k^{\mathrm{l}}, f_c)^H \left(\boldsymbol{R}_k^{\mathrm{l}}\right)^{-1} \boldsymbol{d}(\theta_k^{\mathrm{l}}, f_c)}, \quad (8)$$

$$\boldsymbol{w}_k^{\mathrm{r}} = \frac{\left(\boldsymbol{R}_k^{\mathrm{r}}\right)^{-1} \boldsymbol{d}(\theta_k^{\mathrm{r}}, f_c)}{\boldsymbol{d}(\theta_k^{\mathrm{r}}, f_c)^H \left(\boldsymbol{R}_k^{\mathrm{r}}\right)^{-1} \boldsymbol{d}(\theta_k^{\mathrm{r}}, f_c)}, \quad (9)$$

where θ_k^{l}, θ_k^{r} are the angles at which both the beams are directed. Hence, boresight axis of the receiver is located at an angle $\theta_k^{\mathrm{b}} = \frac{\theta_k^{\mathrm{l}} + \theta_k^{\mathrm{r}}}{2}$. In practice, the covariance matrices $\boldsymbol{R}_k^{\mathrm{l}}$ and $\boldsymbol{R}_k^{\mathrm{r}}$ are not known at the receiver apriori. Therefore, they are approximated using the sample covariance matrices $\widehat{\boldsymbol{R}_k^{\mathrm{l}}}$ and $\widehat{\boldsymbol{R}_k^{\mathrm{r}}}$.

We evaluate the sum and the difference of the absolute values of the complex outputs at the two beamformers and send these measurements to the monopulse processor for the decision making about the angular location of the target.

$$y_k^{\mathrm{s}}[n] = \mathrm{abs}\left\{y_k^{\mathrm{l}}[n]\right\} + \mathrm{abs}\left\{y_k^{\mathrm{r}}[n]\right\}, \quad (10)$$

$$y_k^{\mathrm{d}}[n] = \mathrm{abs}\left\{y_k^{\mathrm{l}}[n]\right\} - \mathrm{abs}\left\{y_k^{\mathrm{r}}[n]\right\}. \quad (11)$$

IV. Tracking Algorithm

A. Initialization

The fusion center has the information about the exact locations of all the receivers. It will initialize the tracking algorithm by making sure that the boresight axes of all the receivers intersect at the same point in space.

B. Monopulse Processing: Local Angular Estimates

After obtaining the measurements from the sum and the difference channels, each of the receivers computes the monopulse ratio

$$M_k[n] = \frac{y_k^{\mathrm{d}}[n]}{y_k^{\mathrm{s}}[n]}. \quad (12)$$

If the $M_k[n]$ is positive, it is highly likely for the target to be present on the left side of the boresight axis. Similarly, a negative $M_k[n]$ indicates the opposite. Therefore, receiver k will adjust its boresight axis appropriately using the following equation

$$\theta_k^{\mathrm{b(new)}} = \theta_k^{\mathrm{b}} + \delta\{M_k[n]\}, \tag{13}$$

where δ is a positive valued design parameter. A larger δ will enable tracking faster moving targets but will also lead to higher steady state errors. However, a smaller δ will increase the convergence time but the steady state errors will be less. Each of the receivers updates its angular estimates and the axis using the above mentioned processing.

C. Fusion Center: Global Location Estimate

The primary function of the fusion center is to combine these decentralized estimates and arrive at a global estimate. We have solved a similar problem for localizing acoustic sources using Cramer-Rao bound [18]. Here, we present a simpler method to combine the decentralized estimates. After obtaining new angular estimates, each of the receivers sends these new updates to the fusion center. Along with the angular estimates, the receivers also send the instantaneous energy of the received signal in the sum channel during that instant.

$$E_k[n] = \left(y_k^{\mathrm{s}}[n]\right)^2. \tag{14}$$

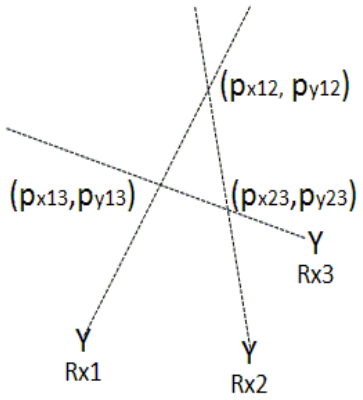

Fig. 4. Polygon formed by the points of intersection of the boresight axes of three receivers.

The fusion center forms a polygon of $\frac{N(N-1)}{2}$ sides by connecting the points of intersection of the updated boresight axes of each of the N receivers (see Fig. 4). The fusion center will decide upon a point inside this polygon to be the global estimate of the target location. Define $\left(p_{x_{ij}}[n], p_{y_{ij}}[n]\right)$ to be the cartesian coordinates of the vertex formed by the intersection of the boresight axes coming out from the i^{th} receiver and the j^{th} receiver. A linear combination of these vertices is chosen as the estimate of the target location

$$(\widehat{p_x}[n], \widehat{p_y}[n]) = \sum_{i=1}^{N} \sum_{j=i+1}^{N} \alpha_{ij}[n] \left(p_{x_{ij}}[n], p_{y_{ij}}[n]\right). \tag{15}$$

We choose the weights $\alpha_{ij}[n]$ to be proportional to the sum of instantaneous energies received from the corresponding receivers and $\sum_{i=1}^{N}\sum_{j=i+1}^{N} \alpha_{ij}[n] = 1$. Therefore,

$$\alpha_{ij}[n] = \frac{E_i[n] + E_j[n]}{\sum_{i'=1}^{N}\sum_{j'=i'+1}^{N}\left(E_{i'}[n] + E_{j'}[n]\right)}. \tag{16}$$

Finally, the fusion center sends this new estimate to all the receivers and guides them to align their axes towards this particular location before the next iteration.

V. Numerical Results

A. Simulated Scenario

In this section, we demonstrate the advantage of the proposed monopulse MIMO tracking system under realistic scenarios. We simulated such a scenario to demonstrate the advantages of this system. First, we describe the locations of the transmitters, receivers, and target on a cartesian coordinate system. The simulated system has two transmitters that are located on the y-axis at distances of $20\mathrm{km}$ and $40\mathrm{km}$ from the origin, respectively. There are three receivers located on the x-axis at the origin, $20\mathrm{km}$ and $40\mathrm{km}$ from the origin, respectively. The receiver at the origin also serves as the fusion center for this setup. The target is initially present at the coordinate $(30, 35)$.

We chose the carrier frequency $f_{\mathrm{c}} = 1\mathrm{GHz}$. We used complex rectangular pulses each with a constant value $\frac{1+\sqrt{-1}}{\sqrt{2}}$ and bandwidth $100\mathrm{MHz}$ for the transmitted baseband waveforms. Therefore, the pulse duration $T = 10^{-8}\mathrm{s}$. The pulse repetition interval $T_{\mathrm{R}} = 4\mathrm{ms}$. We further had two samples per pulse duration (Nyquist rate). We ran the simulation for $2\mathrm{s}$. Hence, we had 500 pulses from each transmitter. The target is airborne and moving with a constant velocity of $(0.25, 0.25)\,\mathrm{km/s}$. There are six complex numbers $\{a_{11}, a_{12}, a_{13}, a_{21}, a_{22}, a_{23}\}$ describing the attenuation experienced by the signals. It is important to realistically model these attenuations. They were independently generated from one pulse to another using zero mean complex normal random variables with their variances chosen from the set $\{0.15, 0.3, 0.45, 0.6, 0.75, 0.9\}$. The a_{ik} corresponding to the antenna pair that are the closest to the target got the higher values and vice versa. We assumed the additive noise at every element of the receiver array is uncorrelated zero mean complex Gaussian distributed with variance σ^2. The received powers are different at different receivers because the attenuations a_{ik} do not have the same variances. Therefore, we evaluate the overall signal to noise ratio (SNR) by computing the average. For a noise variance of $\sigma^2 = 0.1$, SNR=12.3dB. We further assumed the noise to be stationary. The noise variance was estimated from a training data set of 50 samples. We assumed that the target returns were not present in the training samples that were used. We independently generated the noise from one time sample to another. The two beams at each receiver were generated using $L = 10$ element linear arrays and they were made to point 5 degrees on either side of the boresight axis. The $-3\mathrm{dB}$

beamwidth of these beams is approximately 12 degrees. We chose the parameter $\delta = 0.25$ degrees in our algorithm.

B. Spatial Diversity

We first demonstrate the spatial diversity offered by monopulse MIMO radar with widely separated antennas by comparing this system with monopulse SISO radar. Since a single receiver monopulse tracking radar can only track the angular location of the target, we shall compare only the angle errors of the SISO and MIMO monopulse radars. For SISO radar, we assumed only the first transmitter $(0, 20)$ and the first receiver $(0, 0)$ to be present. First, we assumed that the initial estimate of the target location for 2x3 MIMO radar is far from the actual location at $(32, 32)$. Hence, the initial estimate was at a distance of 3.61km from the actual location. The same initial estimate was also used for SISO radar and it corresponds to an initial angular error of 4.3987 degrees. In order to make the comparison fair, we deliberately increased the transmit power per antenna for the SISO system to make the overall transmit power the same. We chose the complex noise variance σ^2 for this comparison to be 0.1. We plotted the angular error as a function of the pulse index. Fig. 5 shows that the MIMO system overcomes a poor initial estimate and manages to track down the target much quicker than the SISO radar. The SISO system takes 60 pulses to come within an angular error of 1 degree. However, the 2x3 MIMO system takes only 20 pulses to reach within the same level of angular error. To obtain good accuracy, we plotted these curves by averaging the results over 100 independent realizations.

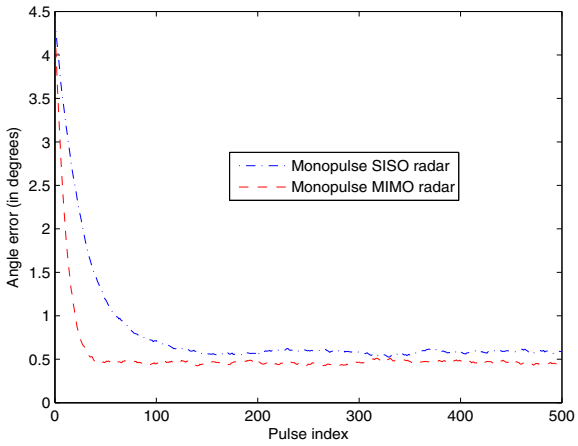

Fig. 5. Comparing the angle error of SISO and MIMO monopulse radars as a function of the pulse index for $\sigma^2 = 0.1$.

Next, we assumed a good initial estimate of $(29.9, 34.9)$ and plotted the average angular errors of both these systems as a function of the complex noise variances. As expected, Fig. 6 shows that the average angular error increases with an increase in the noise variance. MIMO system significantly outperforms the SISO system. The angular error of these systems can further be reduced by using a smaller value of δ. However, if the initial estimate of the target location is poor, a smaller δ would mean that the convergence time of the algorithm would increase. Hence, it is a trade-off between the steady-state error and convergence rate. Note that as the noise variance reduces, the gap between the performances of the systems reduces because the advantage offered by the spatial diversity becomes more relevant when there is more noise. The performance of any monopulse system is independent of the absolute values of the signals of interest. This is an outcome of the fact that we use a ratio in monopulse processing instead of the absolute values of the measured signals in both the channels. As the noise variance increases, we get to see that the improvement offered by the spatial diversity of the MIMO system also increases.

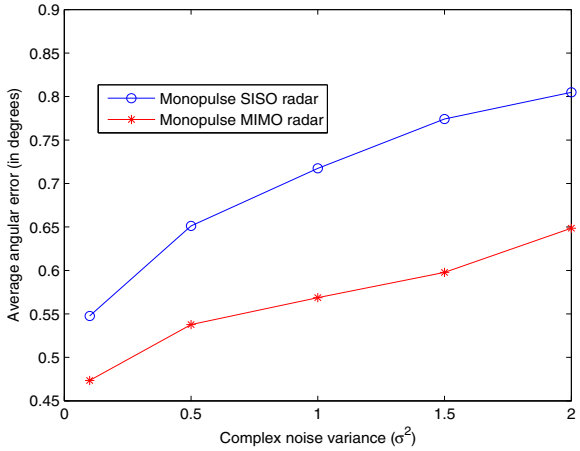

Fig. 6. Comparing the average angle error of SISO and MIMO monopulse radars as a function of the complex noise variance σ^2.

The advantage of the proposed monopulse MIMO radar over monopulse SISO radar stems from the fact that by employing multiple antennas, we are exploiting the fluctuations in the target RCS values with respect to the angle of view. Even if the RCS between one transmitter-receiver pair is very small, it is highly likely that the other transmitter-receiver pairs will compensate for it. Also, in our proposed algorithm, the weights are proportional to the received energies. Hence, with high probability, a transmitter-receiver pair with high RCS value will contribute significantly to the received energy at that particular receiver.

Along with tracking the angular location of the target, the exact coordinates of the target location can also be estimated by evaluating the points of intersection of the boresight axes coming from all the receivers. Since this processing is possible only for monopulse systems with multiple receivers, in the following simulations, we show the localizing abilities of 2x3 MIMO radar under different challenging scenarios.

C. Rapidly Maneuvering Airborne Target

A clever target would change its direction of travel at high velocities to reduce the detectability and to confuse the tracking radar. Hence, it is extremely important to track a rapidly maneuvering airborne target. In order to check the

performance of the algorithm in this scenario, we increased the velocity of the target to $(2.5, 0.833)\,\mathrm{km/s}$ and further made the target change its direction at two different locations over a time span of $8\mathrm{s}$. These high velocities are a feature of the next generation hypersonic missiles. We see from Fig. 7 that the radar system keeps track of the target inspite of the very high velocities and direction changes. The noise variance $\sigma^2 = 0.1$ for this simulation. This corresponds to an SNR of $12.3\mathrm{dB}$.

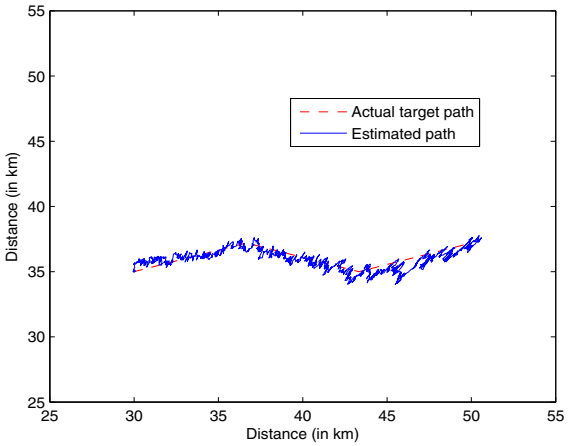

Fig. 7. Monopulse MIMO tracker for a rapidly maneuvering airborne target for $\sigma^2 = 0.1$.

D. Maneuvering Ground Target

Ground targets move at lesser velocities when compared with the airborne targets we have considered so far. However, ground targets have the flexibility to change directions at sharp angles. They can sometimes change their direction by 90 degrees. This poses an important challenge to the tracking system. In Fig. 8, we simulated a ground target moving at a velocity of $(25, 25)\,\mathrm{m/s}$ and completely changing directions at three different locations. Since the target moves slower than an airborne target, we chose the pulse repetition rate $T_{\mathrm{R}} = 0.4\mathrm{s}$ for the simplicity of numerical simulations. We see that the tracker follows the target at each of these locations inspite of the sharp angle changes and the reduction of pulse repetition frequency.

VI. Conclusion

We have proposed a MIMO radar system with monopulse receivers. We used Capon beamforming to generate the beams of the monopulse receivers. Further, we developed a tracking algorithm for this system. We simulated a realistic scenario to analyze the performance of the proposed system. We demonstrated the advantages offered by this system over conventional single antenna monopulse tracking radar. This advantage is a result of the spatial diversity offered by distributed MIMO radar systems. We also showed that the proposed system keeps track of a rapidly maneuvering airborne and ground targets. In future work, we will perform an asymptotic error analysis and develop performance bounds for the proposed tracking algorithm. We will also use real data to demonstrate the advantages of the proposed system.

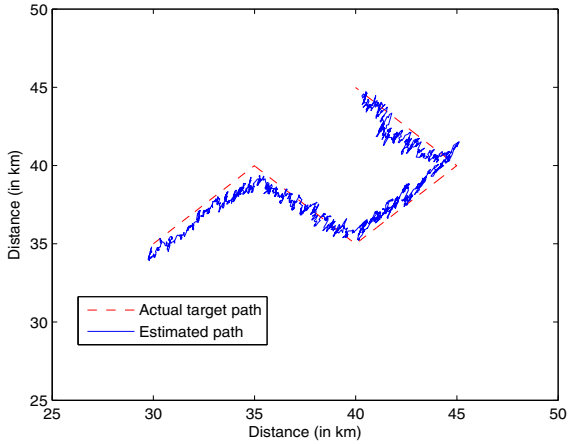

Fig. 8. Monopulse MIMO tracker for a maneuvering ground target for $\sigma^2 = 0.1$.

References

[1] A. M. Haimovich, R. S. Blum, and L. J. Cimini, "MIMO radar with widely separated antennas," *IEEE Signal Process. Mag.*, vol. 25, pp. 116–129, Jan. 2008.

[2] E. Fishler, A. Haimovich, R. S. Blum, L. J. Cimini, D. Chizhik, and R. A. Valenzuela, "Spatial diversity in radars-models and detection performance," *IEEE Trans. Signal Process.*, vol. 54, pp. 823–838, Mar. 2006.

[3] S. Gogineni and A. Nehorai, "Polarimetric MIMO radar with distributed antennas for target detection," *IEEE Trans. Signal Process.*, vol. 58, Mar. 2010.

[4] ——, "Polarimetric MIMO radar with distributed antennas for target detection," in *Proc. 43rd Asilomar Conf. Signals, Syst. Comput.*, Pacific Grove, CA, Nov. 2009.

[5] J. Li and P. Stoica, "MIMO radar with colocated antennas," *IEEE Signal Process. Mag.*, vol. 24, pp. 106–114, Sep. 2007.

[6] J. Li, P. Stoica, L. Xu, and W. Roberts, "On parameter identifiability of MIMO radar," *IEEE Signal Process. Lett.*, vol. 14, pp. 968–971, Dec. 2007.

[7] M. Skolnik, *Radar handbook*. Mcgraw Hill Companies, 2008.

[8] D. R. Rhodes, *Introduction to Monopulse*. New York: McGraw-Hill Book Co., 1959.

[9] S. M. Sherman, *Monopulse principles and techniques*. Dedham, MA: Artech House, Inc., 1985.

[10] W. D. Blair and M. Brandt-Pearce, "Unresolved Rayleigh target detection using monopulse measurements," *IEEE Trans. Aerosp. Electron. Syst.*, vol. 34, pp. 543–552, Apr. 1998.

[11] A. J. Rainal, "Monopulse radars excited by Gaussian signals," *IEEE Trans. Aerosp. Electron. Syst.*, vol. 2, pp. 337–345, May 1966.

[12] S. Gogineni and A. Nehorai, "Monopulse MIMO radar for target tracking," *in revision for IEEE Trans. Aerosp. Electron. Syst.*

[13] P. Swerling, "Probability of detection for fluctuating targets," *IRE Trans. Inf. Theory*, vol. 2, pp. 269–308, Apr. 1960.

[14] F. Mcnolty and E. Hansen, "Some aspects of Swerling models for fluctuating radar cross section," *IEEE Trans. Aerosp. Electron. Syst.*, vol. 10, pp. 281–285, Mar. 1974.

[15] D. A. Shnidman, "Expanded Swerling target models," *IEEE Trans. Aerosp. Electron. Syst.*, vol. 39, pp. 1059–1069, Jul. 2003.

[16] J. Capon, "High-resolution frequency-wavenumber spectrum analysis," *Proc. IEEE*, vol. 57, pp. 1408–1418, Aug. 1969.

[17] H. Krim and M. Viberg, "Two decades of array signal processing research," *IEEE Signal Process. Mag.*, vol. 13, pp. 67–94, Jul. 1996.

[18] M. Hawkes and A. Nehorai, "Wideband source localization using a distributed acoustic vector-sensor array," *IEEE Trans. Signal Process.*, vol. 5, pp. 1479–1491, Jun. 2003.